

Title No. 119-S14

Modeling Corrosion-Damaged Reinforced Concrete Members

by Siavash Habibi, Anca C. Ferche, and Frank J. Vecchio

In this paper, an analytical approach developed for the structural assessment of corrosion-damaged reinforced concrete (RC) structures is presented. The proposed method, suited for finite element analysis, is compatible with smeared rotating crack models and accounts for uniform and pitting corrosion. Modeling corrosion damage involves accounting for the reduction of the cross-sectional area of reinforcement, bond strength degradation between the reinforcement and concrete, deterioration of the reinforcement mechanical properties, and cracking of concrete in the vicinity of the corroded reinforcement. Numerical models and techniques for simulating corrosion damage were incorporated within the algorithms of a nonlinear finite element analysis program. Validation studies successfully reproduced the responses of published experiments on corroded RC beams. Stochastic simulations were also performed, demonstrating the sensitivity of response quantities to changes in various input parameters. The statistics of the response quantities can also be used for reliability analysis by employing methods such as the first-order reliability method.

Keywords: corrosion; finite element analysis; pitting corrosion; reinforced concrete; stochastic analysis; uniform corrosion.

INTRODUCTION

Reinforced concrete (RC) was and continues to be a widely used material in the construction industry. Generally, it is a durable, economical, and versatile material capable of withstanding severe environments. However, increasingly throughout North America, aging infrastructure is developing signs of distress linked to degradation mechanisms that had not been anticipated in the design phase. The 2019 Canadian Infrastructure Report Card¹ and the 2017 ASCE Infrastructure Report Card² offer comprehensive pictures of the state of public infrastructure in Canada and the United States, respectively. Among the various deterioration mechanisms that can afflict RC structures, corrosion of the embedded steel reinforcement is widely recognized as the major cause of degradation. Structural assessment of the deteriorated infrastructure has a central role in the decision-making process on potential repair or replacement strategies. As such, in recent years, considerable research has been devoted toward the development of deterioration models, most of them focused on the ingress of deleterious factors within the concrete cover, thus attempting to predict the corrosion rate.³ Concomitantly, studies such as those carried out by Yu et al.,⁴ Wang and Liu,⁵ Bhargava et al.,⁶ and Cairns et al.⁷ explored the structural implications of corrosion: reduction of the reinforcing bar diameter, concrete cracking, degradation of bond strength, and deterioration of the mechanical properties of corroded reinforcement.

Notwithstanding the progress in understanding the underlying principles of corrosion and its consequences, there is a need for practical, overarching analytical approaches to assist engineers with the performance assessment of corrosion-damaged structures. The most versatile tool for performance assessment remains finite element (FE) analysis, as it enables the simulation of complex geometries and general types of loading. Among the major factors limiting the use of FE analysis for non-research applications are extensive requirements for the definition of material properties and the calibration of analysis parameters. The work presented in this paper addresses this major research gap by presenting a robust nonlinear FE analysis approach for the assessment of RC elements suffering from reinforcement corrosion.

RESEARCH SIGNIFICANCE

The work presented herein includes the development of a numerical procedure on the macroscale modeling of RC elements suffering from corrosion, compatible with FE analysis frameworks. The proposed procedure encompasses the effects of uniform and pitting corrosion and addresses the inherently substantial uncertainty introduced by corrosion with a stochastic modeling strategy. The validation studies produced results in good agreement with the experimentally measured responses. Considering the numerous aging and defective RC structures within the built environment, it is essential for engineers to have an adequate tool to enable reliable structural assessment.

ANALYTICAL APPROACH

Background

The proposed analytical procedure for modeling corrosion-damaged RC structures is compatible with smeared rotating crack conceptual models for concrete. It was incorporated within the algorithms of the nonlinear FE analysis program, VecTor2,^{8,9} suited for analyzing two-dimensional (2-D) elements. The program employs an incremental total-load, iterative secant-stiffness formulation with the constitutive, compatibility, and equilibrium relationships formulated in terms of the average stresses and average strains. In addition, the local conditions at cracks are explicitly considered. The rotating crack model for concrete is based on the

ACI Structural Journal, V. 119, No. 1, January 2022.

MS No. S-2020-516.R2, doi: 10.14359/51733011, received June 2, 2021, and reviewed under Institute publication policies. Copyright © 2022, American Concrete Institute. All rights reserved, including the making of copies unless permission is obtained from the copyright proprietors. Pertinent discussion including author's closure, if any, will be published ten months from this journal's date if the discussion is received within four months of the paper's print publication.

Modified Compression Field Theory¹⁰ and the Disturbed Stress Field Model.¹¹ Mechanisms such as compression softening, confinement, tension stiffening, tension softening, and shear slip along crack interfaces are some of the behavioral mechanisms considered.

The addition of corrosion-modeling capabilities involved the implementation of numerical models for the corrosion rate, cover cracking, bond strength degradation, and deterioration of the mechanical properties of corrosion-damaged reinforcement, as detailed in the subsequent sections. An important aspect of the program's applicability for the analysis of corrosion-affected elements is the minimal need for calibration. The default behavioral models described are suitable for the majority of analyses as they have been extensively verified against a broad range of structures.

Corrosion rate

The corrosion rate is the parameter that reflects the progress of corrosion-induced damage, giving a quantitative description of corrosion propagation. It is typically described as the loss of metal per unit of surface area per unit of time (mm/year) or as current density (1 $\mu\text{A}/\text{cm}^2$). The proposed formulation requires the corrosion rate expressed in mm/year, as well as the age in days of the RC element, as an input for corrosion analysis.

For a reliable assessment of corrosion-damaged RC elements, the corrosion rate is one of the most influential input parameters.¹² The reduction in the diameter of the reinforcement, the bond strength, the area of the pits formed over the reinforcing bars, and the extent of cover cracking are all influenced by the corrosion attack penetration, which is directly proportional to the corrosion rate. Approaches for predicting the corrosion rate range from empirical-based models¹³ to solely mathematical models,¹⁴ and from time-invariant models¹⁵ to time-variant ones.¹⁶

Assuming homogenous corrosion, Andrade et al.¹⁷ employed Faraday's law and empirical data to calculate the conversion from current density (1 $\mu\text{A}/\text{cm}^2$) to loss of metal per unit of surface area per unit of time (mm/year), as per Eq. (1)

$$1.0 \mu\text{A}/\text{cm}^2 = 0.0116 \text{ mm/year} \quad (1)$$

Therefore, the following relationship was derived to express the residual diameter of a corroded bar, $d_b(t)$, as a function of the current density

$$d_b(t) = d_{b0} - 0.0232 \cdot i_{corr} \cdot t \text{ (mm)} \quad (2)$$

where d_{b0} is the initial bar diameter, mm; i_{corr} is the corrosion current density, $\mu\text{A}/\text{cm}^2$; and t is the period of active corrosion, years.

Equations (1) and (2) were implemented within the program VecTor2 to calculate the residual bar diameter for reinforcement affected by uniform corrosion. Consideration was also given to time-variant corrosion-rate approaches such as the Liu and Weyers¹⁶ model. The "Corrosion rate"

section in the Appendix* shows a comparison between the Liu and Weyers¹⁶ model, the time-invariant model described by Eq. (1) and (2), and experimental results from studies conducted by Rodriguez et al.¹⁸ and El Maaddawy and Soudki.¹⁹ The time-invariant model matched the experimental results more accurately than the Liu and Weyers¹⁶ model; therefore, it was adopted in the proposed formulation.

The formulation suggested by Stewart and Al-Harthy²⁰ was employed to calculate the reduced steel cross-sectional area in the case of pitting corrosion. A pitting factor, R , defined as the ratio of the maximum pit depth to the corrosion penetration calculated based on the uniform corrosion, is used to define the degree of pitting, as per Eq. (3). For the analysis of pitting corrosion, the pitting factor R , the mean corrosion rate (mm/years), and the time since corrosion initiation in days are required as input data.

$$R = p / P_{avg} \quad (3)$$

where R is the pitting factor; p is the maximum pit depth, mm; $P_{avg} = 0.0116 \cdot i_{corr} \cdot t$ is the corrosion penetration calculated based on the uniform corrosion; i_{corr} is the current density, $\mu\text{A}/\text{cm}^2$; and t is the time since corrosion initiation in years.

The cross-sectional area of the pit is expressed in Eq. (4), based on the pit configuration shown in the Appendix (Fig. A.3).

$$A_{pit} = \begin{cases} A_1 + A_2 & p \leq \frac{D_0}{\sqrt{2}} \\ \frac{\pi D_0^2}{4} - A_1 + A_2 & \frac{D_0}{\sqrt{2}} \leq p \leq D_0 \text{ (mm}^2\text{)} \\ \frac{\pi D_0^2}{4} & p \geq D_0 \end{cases} \quad (4)$$

where

$$b = 2p \sqrt{1 - \left(\frac{p}{D_0}\right)^2} \quad A_1 = 0.5 \left[\theta_1 \left(\frac{D_0}{2}\right)^2 - b \left| \frac{D_0}{2} - \frac{p^2}{D_0} \right| \right]$$

$$A_2 = 0.5 \left[\theta_2 p^2 - b \frac{p^2}{D_0} \right] \quad \theta_1 = 2 \arcsin \left(\frac{b}{D_0} \right) \quad \theta_2 = 2 \arcsin \left(\frac{b}{2p} \right)$$

D_0 is the initial bar diameter, mm.

Cover cracking

The service life of a corroding RC structure is typically divided into three stages. In the beginning, the high alkalinity of hydration products results in the formation of a protective layer of iron hydroxide around the reinforcement. In the first stage, the chloride or carbon dioxide content of the concrete cover reaches a threshold value at which the alkalinity of the concrete pore solution reduces to the point where the protective iron hydroxide layer is destabilized, exposing the surface of the reinforcement to corrosion. Once

*The Appendix is available at www.concrete.org/publications in PDF format, appended to the online version of the published paper. It is also available in hard copy from ACI headquarters for a fee equal to the cost of reproduction plus handling at the time of the request.

sufficient oxygen and moisture are present, the first stage ends, and the reinforcement starts to corrode. The second stage can be simulated by employing Fick's law of diffusion. The solid iron is transformed into ferrous or ferric ions accumulating in the pores of the interfacial zone of the steel-concrete, referred to as the diffusion zone. Thus, no stresses develop in the cover concrete during this stage. Once the diffusion zone is filled with corrosion products, the third stage begins. During this stage, tensile stresses develop in the cover concrete due to corrosion of the reinforcement. Radial cracks form and propagate in the concrete surrounding the reinforcement until a serviceability limit state, such as the spalling or delamination of the cover concrete, occurs.^{5,21,22}

The work presented in this paper is focused on the third stage. Corrosion-induced cracking is treated as an initial strain generated in the elements in the vicinity of a corroded reinforcing bar. The first and second stages are not included for the following reasons:

1. The duration of the first and second stages can be treated as a time shift in the service life of a corroded RC member.
2. There is significant disagreement in the literature regarding the reported volumes of the porous zone around the reinforcement.
3. The first stage is typically bypassed in the accelerated corrosion tests by adding a chlorine compound to the concrete mixture exceeding the minimum threshold value required for steel passivation.

Two models available in the literature were implemented within the proposed formulation: Pantazopoulou and Papoulia²¹ and Wang and Liu.⁵ The Appendix section "Cover cracking models implementation" details the implementation of these two models.

Bond strength

Bond stresses between steel and concrete are transferred by adhesion and friction and by bearing of the deformations of the reinforcing bar on the concrete. Adhesion and friction are severely reduced when the corrosion products accumulate around a reinforcing bar. Moreover, cracking of the cover reduces the confining action of the concrete. As a result, the bond and anchorage between the concrete and the reinforcement deteriorate. Pullout tests on corroded bars have shown that the bond strength increases slightly before cracking of the concrete cover.²³ This is attributed to an increase in the pressure applied to the concrete by corrosion products, which adds to the confining action provided by the concrete. However, once the concrete reaches its tensile strength, the bond strength reduces greatly. Quantifying the bond strength between the reinforcement and the concrete is essential for the assessment of the residual strength of corrosion-damaged RC structural members.⁶

Four empirical bond strength reduction models for corroded deformed bars were chosen from the available literature and implemented within VecTor2: Val et al.,²⁴ Chung et al.,²⁵ Feng et al.,²⁶ and El Maaddawy et al.²⁷ The models are summarized in the Appendix section "Bond strength models implementation." All the models provide a reduction factor for the bond strength of a corroded reinforcing bar. The bond models in VecTor2 were updated to

include the bond strength reduction factor, R . The default bond stress-slip model in VecTor2 is the Eligehausen model and consists of a multilinear bond stress-slip relationship described by an ascending nonlinear branch, followed by a constant bond stress plateau, a linearly declining phase, and a residual stress phase.⁹ The analyses presented in this paper used the Eligehausen model for the bond stress-slip relationship in conjunction with the bond strength reduction models investigated.

The implemented bond strength reduction models were verified against pullout tests performed by Al-Sulaimani et al.²³ The Feng et al.²⁶ model gave the most accurate predictions; however, due to the large variability associated with bond strength, the more conservative models provided by Val et al.²⁴ and Chung et al.²⁵ are recommended for use. The results are given in the Appendix section "Bond strength models implementation" and Fig. A.11.

Mechanical properties of corrosion-damaged reinforcement

Reinforcing bars subjected to local or pitting corrosion may suffer a loss of strength or ductility. The consequences of uniform corrosion were addressed by reducing the cross-sectional area of the corroded bar, reducing the bond strength, and calculating the corresponding strains in the concrete elements in the vicinity of the reinforcing bar. However, the nature of the pitting attack is substantially different from that of uniform corrosion. The oxidation products of pitting corrosion are less expansive to the extent that no signs of longitudinal cracking might become visible prior to significant section loss.⁷

In the proposed formulation, the mechanical properties of a corroded truss element subjected to pitting corrosion were updated using the Cairns et al.⁷ model

$$f_y = (1 - \alpha_y \cdot Q_{corr}) f_{y0} \text{ (MPa)} \quad (5)$$

$$f_u = (1 - \alpha_u \cdot Q_{corr}) f_{u0} \text{ (MPa)} \quad (6)$$

$$\epsilon_u = (1 - \alpha_1 \cdot Q_{corr}) \epsilon_{u0} \quad (7)$$

where f_{y0} , f_{u0} , and ϵ_{u0} are the yield strength, ultimate strength, and ultimate strain of a noncorroded bar; f_y , f_u , and ϵ_u are the yield strength, ultimate strength, and ultimate strain of a corroded bar; Q_{corr} is the cross-section loss expressed as a percentage of the original cross section; and α_y , α_u , and α_1 are the empirical coefficients.

A noticeable scatter was observed in the reported values of the empirical coefficients α_y , α_u , and α_1 . Nonetheless, for pitting corrosion, the coefficients suggested by Du²⁸ were incorporated in VecTor2. As such, for Q_{corr} ranging from 0 to 18%, $\alpha_y = 0.015$, $\alpha_u = 0.015$, and $\alpha_1 = 0.039$.

DETERMINISTIC MODELING OF CORRODED RC BEAMS

The accuracy of the corrosion damage models implemented in VecTor2 and the analytical procedure was verified

by analyzing the beam elements with corroded reinforcement tested in the literature. Two types of analyses were performed: deterministic and stochastic. The spatial variability of cross-sectional loss due to corrosion was not considered in the deterministic analyses, whereas in the stochastic simulations, such variability was incorporated in the FE models by using Monte Carlo sampling. This section discusses the deterministic analyses.

The default VecTor2 behavioral models were used. For additional information on the behavioral models, the reader is referred to Wong et al.⁹ For each specimen, the cylinder compressive strength, tensile strength, and initial tangent modulus of the concrete, as well as the yield strength, ultimate strength, and modulus of elasticity of the reinforcement steel, were specified according to the values reported. In cases where one or more of these material properties were not reported, reasonable assumptions, mentioned in the following sections, were made. VecTor2 default values were used for other material properties.

Table 1—Mechanical properties of concrete and reinforcement: Azad et al.²⁹ beams

Beam series	Concrete	10 mm reinforcing bar		12 mm reinforcing bar	
	f'_c , MPa	f_y , MPa	f_{ur} , MPa	f_y , MPa	f_{ur} , MPa
BT1	45.8	520	551	590	700
BT2	36.3	520	551	590	700
BT3	46.5	520	551	590	700
BT4	46.1	520	551	590	700

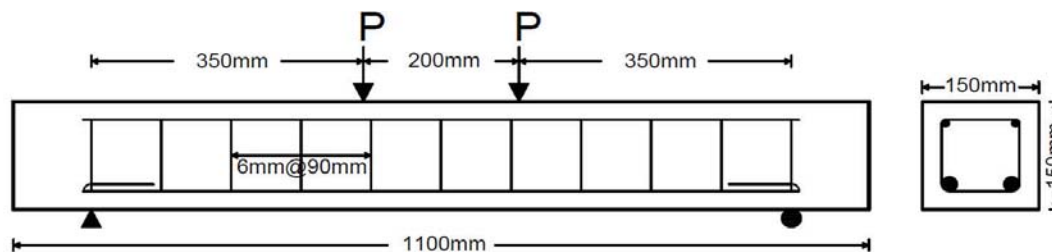
Note: 1 MPa = 145 psi; 1 mm = 0.04 in.

Azad et al.

Azad et al.²⁹ tested 28 RC beams to investigate the effects of varying degrees of reinforcement corrosion on the flexural behavior of RC beams. The variables of the tests were the bar diameter, clear cover to the tension reinforcement, corrosion current density, and duration of the tests. The mechanical properties of the concrete and the reinforcement are given in Table 1. The beams were 1100 mm long and had a 150 mm square cross section. Double-legged 6 mm diameter stirrups, spaced 90 mm apart, were provided in each beam. Two 8 mm diameter deformed bars with a 36 mm clear cover were placed at the top of the beams as compression reinforcement. The tension reinforcement consisted of two 10 or 12 mm diameter bars as detailed in the Appendix section “Azad et al. beam specimens details.” The geometry of a typical test specimen is depicted in Fig. 1(a). Corrosion of the reinforcement occurred in accelerated conditions.

FE models of the beams were created using FormWorks, the preprocessor program for VecTor2. Except for the material properties summarized in Table 1, the remaining input parameters were left as the default VecTor2 values. The reinforcement layout, together with the mesh and support conditions, are shown in Fig. 1(b). The FE mesh had dimensions of 10 x 10 mm for every region. The stirrups in the out-of-plane direction were modeled as smeared reinforcement. In-plane tension, compression, and transverse reinforcement were modeled with 311 truss elements. The bond between the concrete and the corroded truss elements was modeled with link elements over the entire length of the tension reinforcement.

The loss of cross-sectional area of the reinforcement was calculated based on the applied corrosion current density,



(a) Geometry of Azad et al.²⁹ beams (Note: 1 mm = 0.04 in.)

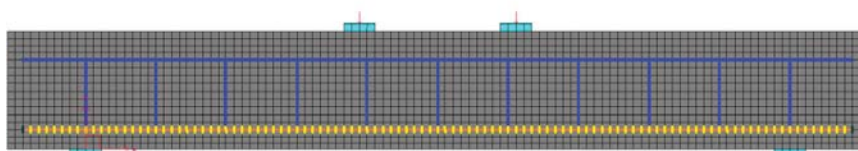


Fig. 1—Azad et al.²⁹ typical specimens: geometry and finite element model.

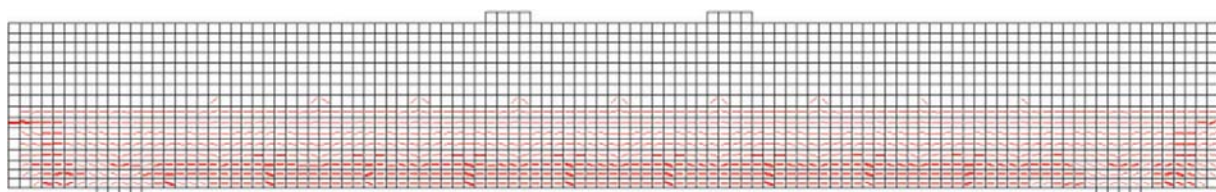


Fig. 2—Typical corrosion-induced crack pattern for Azad et al.²⁹ beam.

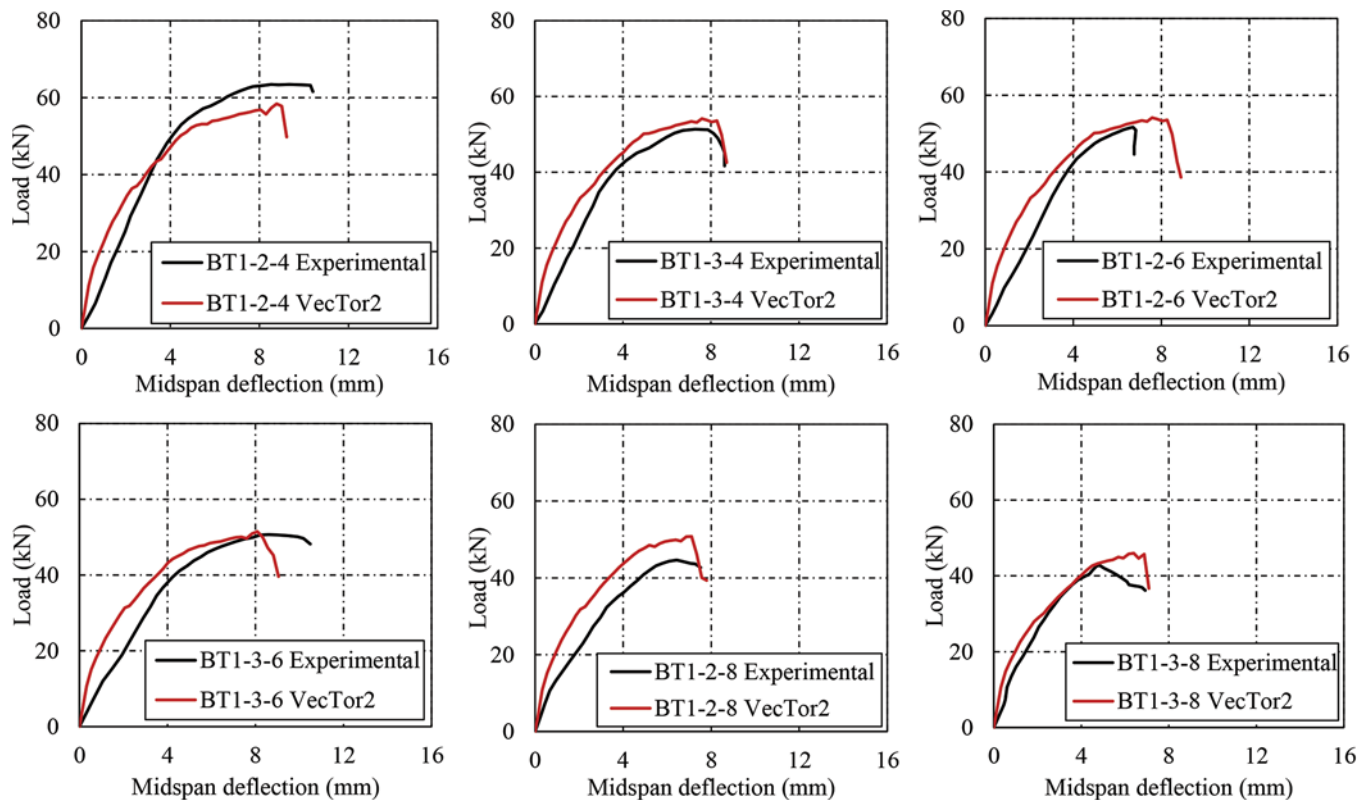


Fig. 3—Experimental versus analytical load-deflection responses for Azad et al.²⁹ specimens. (Note: 1 kN = 225 lbf; 1 mm = 0.04 in.)

using Eq. (2). The Feng et al.²⁶ and Pantazopoulou and Papouli²¹ models were used to calculate the bond strength reduction factor and the cracking of the cover concrete, respectively. A typical corrosion-induced crack pattern is shown in Fig. 2. The increase in the volume of the corroded bars generated tensile stresses up to 163 MPa in the transverse reinforcement.

A monotonic nodal displacement with increments of 1.0 mm was applied to the FE models at the locations shown in Fig. 1. The experimental load-displacement curves were provided for only six out of the 24 corroded beams by Azad et al.²⁹ Load-deflection responses predicted by VecTor2, along with the experimental ones, are shown in Fig. 3 for these six beams. Generally, the responses were captured well by the FE analyses in terms of the ultimate load and displacement capacity. The analytical stiffnesses of the beams, however, were slightly overestimated compared with the experimental results. This may be due to the overestimation of the concrete modulus of elasticity (taken as $3320\sqrt{f'_c} + 6900$ MPa) or the modulus of elasticity of the reinforcement (estimated as 200,000 MPa). These assumptions were necessary as data was not reported.

Summarized in Table 2 are the experimental ultimate loads, $P_{u, \text{expt}}$; the analytical ultimate loads, $P_{u, \text{VecTor2}}$; and the ratios of the analytical-to-experimental ultimate loads for all the specimens. The FE analyses accurately predicted the specimens' capacity, with the ratios of the analytical-to-experimental ultimate loads having a mean of 1.05 and a coefficient of variation (COV) of 17.4%.

The analytical results were found to be highly sensitive to the choice of the bond strength reduction model. Shown in

Fig. 4 are the load-deflection analytical responses calculated for beam specimen BT1-2-4 with each of the implemented bond strength reduction models. The El Maaddawy et al.²⁷ model predicted the smallest reduction in the bond strength among the four models, with a 46% reduction. Tensile stresses higher than the yield strength of the tension reinforcement were developed over a significant length of the beam. As a result, the FE model had a ductile response with a clearly defined yield plateau. The Chung et al.²⁵ and Feng et al.²⁶ models predicted 79% and 82% reductions in the bond strength, respectively. The Val et al.²⁴ model predicted a 90% bond strength reduction, resulting in bond breakdown at an early stage of the loading. Debonding of the reinforcement was found to be an influential mechanism for the response of flexural-critical specimens. For the Azad et al.²⁹ beams, the analyses employing the Feng et al.²⁶ and Chung et al.²⁵ bond strength reduction models reproduced the experimental results more accurately. However, the disparate values of the bond strength reduction factors emphasize the need for further research to better characterize the degree of bond degradation in RC members affected by corrosion.

The cover cracking models did not have a significant influence on the overall response of the beams. The Wang and Liu⁵ model predicted smaller tensile strains induced in the concrete surrounding the corroded bars compared with the values calculated by the Pantazopoulou and Papouli²¹ model. Nevertheless, this discrepancy did not translate into a notable difference in the calculated analytical responses. The concrete elements severely affected by corrosion were the ones located below the tension reinforcement. During the monotonic loading phase, these elements were subjected to

Table 2—Experimental versus calculated ultimate loads of Azad et al.²⁹ beams

Beam	$P_{u, test}$, kN	$P_{u, VecTor2}$, kN	$P_{u, VecTor2}/P_{u, test}$	Beam	$P_{u, test}$, kN	$P_{u, VecTor2}$, kN	$P_{u, VecTor2}/P_{u, test}$
BT1-C	66.51	63.16	0.95	BT3-C	67.20	55.94	0.83
BT1-2-4	61.02	58.30	0.96	BT3-2-4	62.40	51.60	0.83
BT1-3-4	58.00	54.22	0.93	BT3-3-4	58.23	49.36	0.85
BT1-2-6	59.77	54.22	0.91	BT3-2-6	56.46	49.36	0.87
BT1-3-6	52.29	51.03	0.98	BT3-3-6	53.03	46.54	0.88
BT1-2-8	44.69	50.93	1.14	BT3-2-8	52.11	47.40	0.91
BT1-3-8	37.03	46.12	1.25	BT3-3-8	37.71	43.33	1.15
BT2-C	84.57	86.90	1.03	BT4-C	75.03	83.88	1.12
BT2-2-4	72.91	64.52	0.88	BT4-2-4	68.74	73.07	1.06
BT2-3-4	68.40	64.26	0.94	BT4-3-4	62.46	70.19	1.12
BT2-2-6	59.60	61.80	1.04	BT4-2-6	57.26	70.19	1.23
BT2-3-6	60.29	59.56	0.99	BT4-3-6	51.31	67.70	1.32
BT2-2-8	50.74	59.67	1.18	BT4-2-8	51.43	69.79	1.36
BT2-3-8	48.51	59.90	1.03	BT4-3-8	43.26	64.03	1.48
						Mean	1.05
						COV	17.4%

Note: 1 kN = 225 lbf.

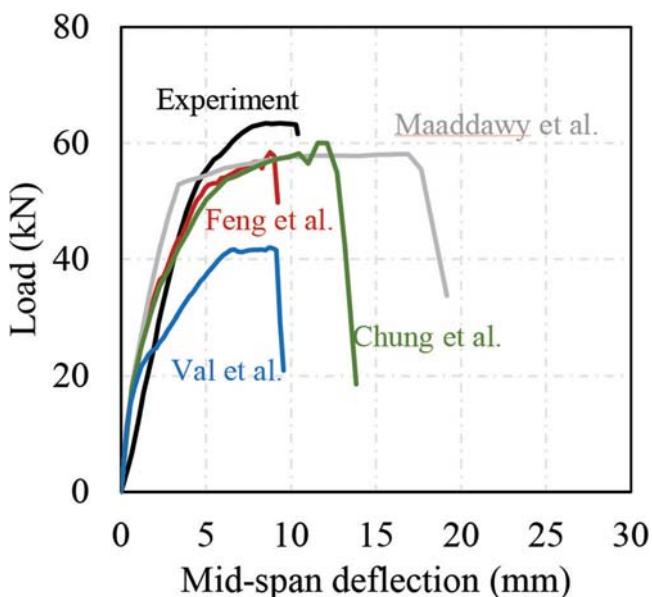


Fig. 4—Bond strength reduction model influence on analytical response of BT1-2-4 beam. (Note: 1 kN = 225 lbf; 1 mm = 0.04 in.)

the highest tensile strains in the beam. Whether corrosion had occurred or not, they would experience high levels of strain during the loading protocol. Thus, except for a serviceability limit state, cracking of the concrete cover is not expected to significantly influence the capacity of a corroded flexural-critical member.

EI Maaddawy et al.

EI Maaddawy et al.³⁰ studied the effect of sustained loading and simultaneous corrosion on the flexural behavior of RC beams. The beams were identical in size, each measuring

Table 3—Mechanical properties of reinforcing bars: EI Maaddawy et al.³⁰ beams

—	Bar type	D, mm	f_y , MPa	f_u , MPa
Tensile reinforcement	Deformed	16	450	585
Compression reinforcement	Smooth	8	340	500
Stirrups	Smooth	8	340	500

Note: 1 MPa = 145 psi; 1 mm = 0.04 in.

152 x 254 x 3200 mm, and had similar material properties. The only design variable was the corrosion time. Two No. 15 Grade 60 bars and two 8 mm diameter smooth bars were used as tension and compression reinforcement, respectively. Stirrups were double-legged 8 mm diameter smooth bars, spaced 80 mm apart in the shear span and 333 mm in the constant moment region. For each beam, 2.25% chloride by weight of cement was added to the concrete in the lower middle area over a 1400 mm length and a 100 mm height. Thus, only the portion of the tension reinforcement within the salted zone was expected to corrode. The remaining length of the tension bars and the whole length of the compression and transverse reinforcement were protected against corrosion by epoxy coating. The mechanical properties of the reinforcement are given in Table 3. The average cylinder compressive strengths of the salted and unsalted concrete were 40 and 41 MPa, respectively.

A direct electrical current with an intensity of 215 mA, equivalent to a current density of 150 $\mu\text{A}/\text{cm}^2$, was used to accelerate the corrosion of the tension bars. One of the beams was used as the control specimen, with no corrosion. The remaining eight beams were divided into two groups: group CN, kept unloaded during the accelerated corrosion period, and group CS, corroded under a sustained loading that caused a midspan moment equal to 60% of the yield

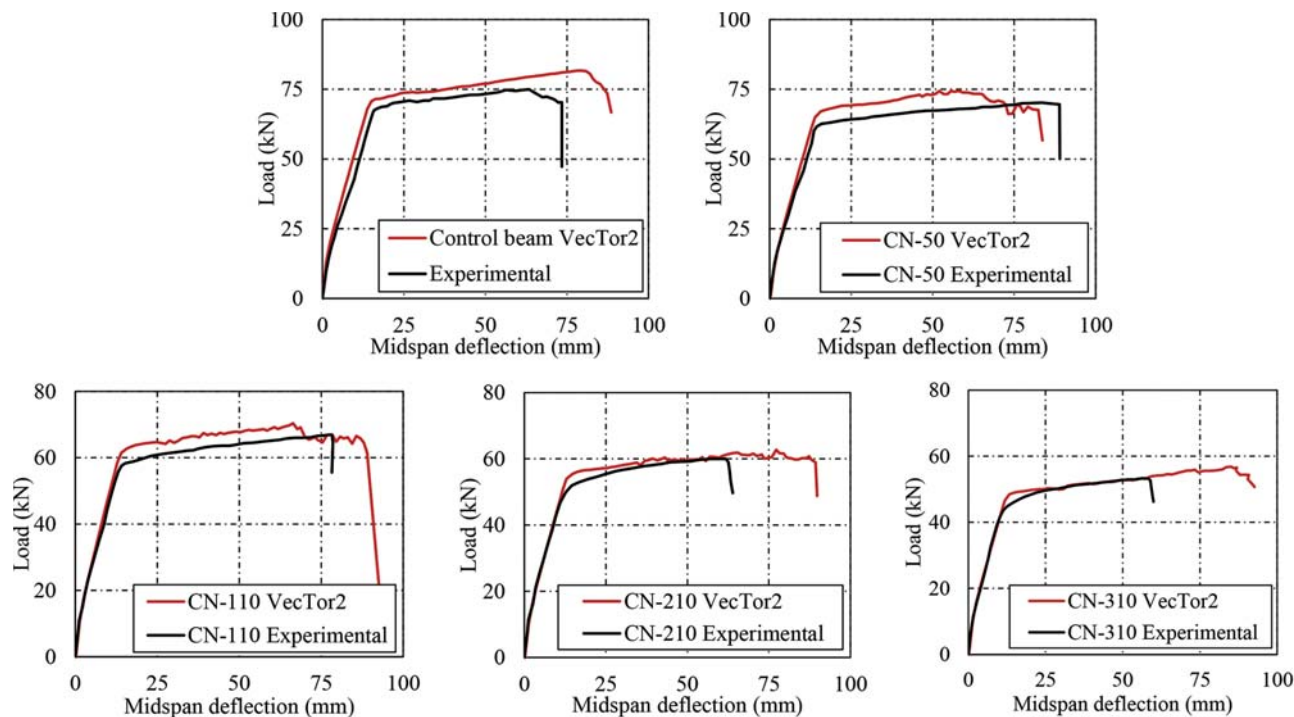


Fig. 5—Experimental versus analytical load-deflection responses for El Maaddawy et al.³⁰ specimens. (Note: 1 kN = 225 lbf; 1 mm = 0.04 in.)

moment. After 50, 110, 210, and 310 days of accelerated corrosion, the flexural strengths of the beams were examined under four-point bending tests. The beams with sustained loading initially experienced a higher rate of corrosion, resulting in a greater reduction in strength, compared with the beams with no sustained loading. However, the reduction in strength was independent of the sustained loading at high degrees of corrosion.

The FE model was developed with corroded steel assigned as the material type of the middle 1400 mm length of the tension reinforcement. Normal steel was used as the material type for the rest of the reinforcing bars. The stirrups in the out-of-plane direction were smeared uniformly throughout the length of the beams. Only the CN group of beams were considered for the analytical study as the difference in the average mass loss of the corroded reinforcement of the CN and CS beams was deemed negligible. The FE models were loaded with a monotonically increasing nodal displacement with increments of 1.0 mm up to failure.

The analytical load-deflection responses are compared with the experimental responses in Fig. 5. The initial stiffness, ultimate strength, and load that caused the yielding of the tension reinforcement were all captured well by the FE analyses. Larger experimental ultimate deflections were measured for the specimens that experienced 50 and 110 days of corrosion. This may be attributable to the reduction of the tension reinforcement cross-sectional area, resulting in a smaller flexural stiffness. On the other hand, the decreased ductility of the CN-210 and CN-310 beams might be due to the prevailing effect of pitting corrosion in a longer period of corrosion exposure. Overall, the ratios of the analytical-to-experimental ultimate loads had a mean ratio of 1.06 with a COV of 1.67%.

The corrosion-induced cracks reported in the experiments are compared with the cracks simulated for the CN-310 beam in Fig. 6. The analytical models predicted the width of the longitudinal cracks caused by corrosion with reasonable accuracy. The fluctuations in the width of the corrosion cracks, observed in the VecTor2 model, were a result of the confining action of the stirrups.

Du et al.

Du et al.³¹ carried out an experimental program to study the effects of steel corrosion on the failure mode of RC beams. Nineteen RC beams in four groups—very under-reinforced, under-reinforced, balanced, and over-reinforced beams—were constructed and tested to failure. The variables of the tests were the area and the type of the tension reinforcement, the location of the corroded reinforcement, and the degree of corrosion. The mechanical properties of the reinforcing bars are given in Table 4. All the beams had the same dimensions of 150 x 200 x 2100 mm. They were reinforced with 0.56 or 0.87% compression reinforcement, 8 mm diameter stirrups spaced at 150 mm, and 0.87, 1.6, 3.5, or 6.2% tension reinforcement, as summarized in the Appendix section “Du et al. beam specimen details.” Sodium chloride was added to the concrete mixture used in casting the middle 600 mm portion of the beams. The reinforcing bars were corroded by applying a direct current. The current was applied only to the compression, tension, or transverse reinforcement of each specimen located in the salted region, as detailed in the Appendix section “Du et al. beam specimen details.” However, the high electrical conductivity of the chloride-saturated concrete resulted in the corrosion of all the reinforcing bars located in the salted zone. There were no signs of corrosion in the bars located in the unsaturated

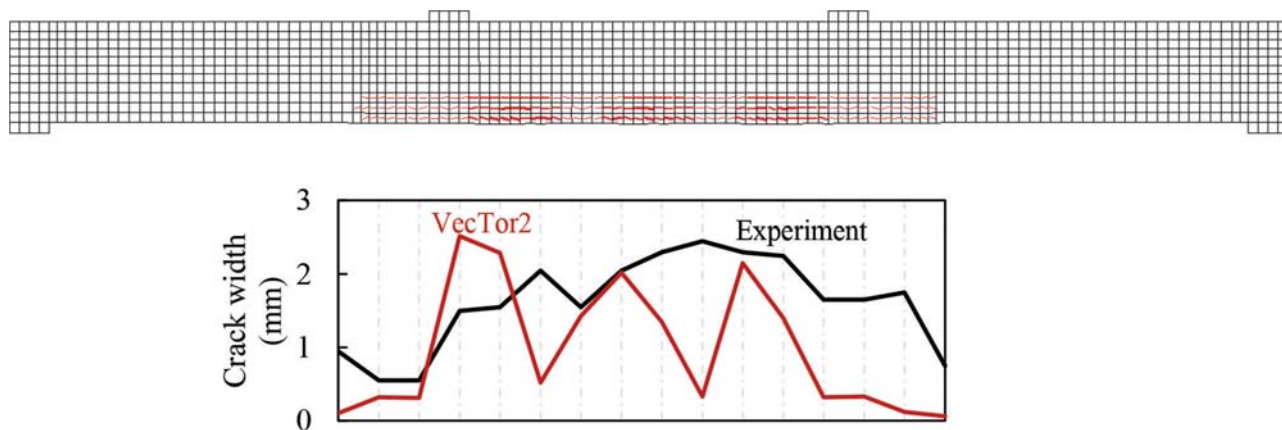


Fig. 6—Experimental versus modeled corrosion-induced cracking. (Note: 1 mm = 0.04 in.)

Table 4—Mechanical properties of reinforcing bars: Du et al.³¹ beams

Type		Smooth	Deformed			
No.		R12	T08	T12	T16	T32
Diameter	mm	12.5	7.91	12.01	15.92	31.61
Yield strength	MPa	385	526	489	529	498
Ultimate strength	MPa	539	619	595	627	604
Elastic modulus	GPa	199	203	202	201	211
Yield strain	$\times 10^{-3}$	1.9	2.6	2.4	2.6	2.5
Hardening strain	$\times 10^{-3}$	25	22	20	19	17
Ultimate strain	$\times 10^{-3}$	203	82	132	116	123

Note: 1 MPa = 145 psi; 1 mm = 0.04 in.

regions. The cross-sectional loss due to corrosion ranged from 2.4 to 11.5% for the tension bars, 6.6 to 13.5% for the compression bars, and 23 to 68% for the stirrups.

The beams were tested to failure under four-point bending with a constant moment span of 300 mm and simply supported conditions. Corrosion caused the over-reinforced beams to fail in a less brittle manner due to either a reduction of the reinforcement cross-sectional area or cracks development within the compression zone of the beams due to corrosion of the compression bars. The under-reinforced beams failed in a less ductile manner because of the reduced ductility of the reinforcement due to pitting corrosion and degradation of the bond between the reinforcement and the concrete. Only 10% corrosion was enough to transform the failure mode of the very under-reinforced beams from ductile to extremely brittle, failing due to the rupture of the corroded tension bars.

The cylinder compressive strength of the concrete was assumed to be 80% of the cube strength. Other concrete material properties were not reported; thus, they were left as the default VecTor2 values. The reinforcing bars were modeled with discrete truss elements. The corroding portion of the reinforcement of each beam was modeled as corroded reinforcement steel material type. A total of 1339 rectangular elements and 315 truss elements were used to model each beam. The corroded reinforcement was connected to the concrete elements using link elements.

The load-deflection responses of the beams are shown in Fig. 7. The very under-reinforced control beam, T280, was modeled twice, assuming perfect and imperfect bonds between the tension reinforcement and the concrete, significantly influencing the ultimate displacement and failure mode. Both analyses captured the peak load well; however, the imperfect bond model resulted in a pronounced reduction in the ultimate displacement caused by premature bond failure of the tension reinforcement. The experimental response of the T280 beam shows a clearly defined yield plateau, while the analytical results assume the imperfect bond did not reach the yielding of the tension reinforcement. Nevertheless, the remaining control specimens were modeled assuming the imperfect bond. For each specimen, the load-deflection curve up to failure was predicted reasonably well by the FE analyses, as shown in Fig. 7.

The corroded beams were modeled using the Feng et al.²⁶ and Pantazopoulou and Papoulia²¹ models. Some discrepancies in the stiffness and ultimate displacement can be observed in the predicted load-deflection responses. Almost every beam failed by crushing of the concrete. As a result of bond failure, the tension reinforcement of the very under-reinforced beams did not yield. In contrast, the tension reinforcement of the under-reinforced and balanced beams reached the yield stress, with negligible slip occurring after yielding. The balanced beam with corroded compression reinforcement, C124, failed by concrete crushing in an early stage of loading mainly due to the reduction of the compression reinforcement area and loss of the composite action. The response of the over-reinforced beams was also accurately estimated by the FE analysis.

STOCHASTIC MODELING OF CORRODED RC BEAMS

In-place inspections of corroded bars revealed significant irregularity and heterogeneity of the spatial distribution of cross-sectional loss due to corrosion, whether uniform or pitting corrosion.⁷ Another example is the beams tested by Yu et al.,⁴ in which the ratio of local cross-section loss to the average section loss varied from 0.2 to 3.5 at different locations along the length of the beams. In addition, although the specimens were subjected to the same corrosive conditions, the average cross-sectional loss of each reinforcing

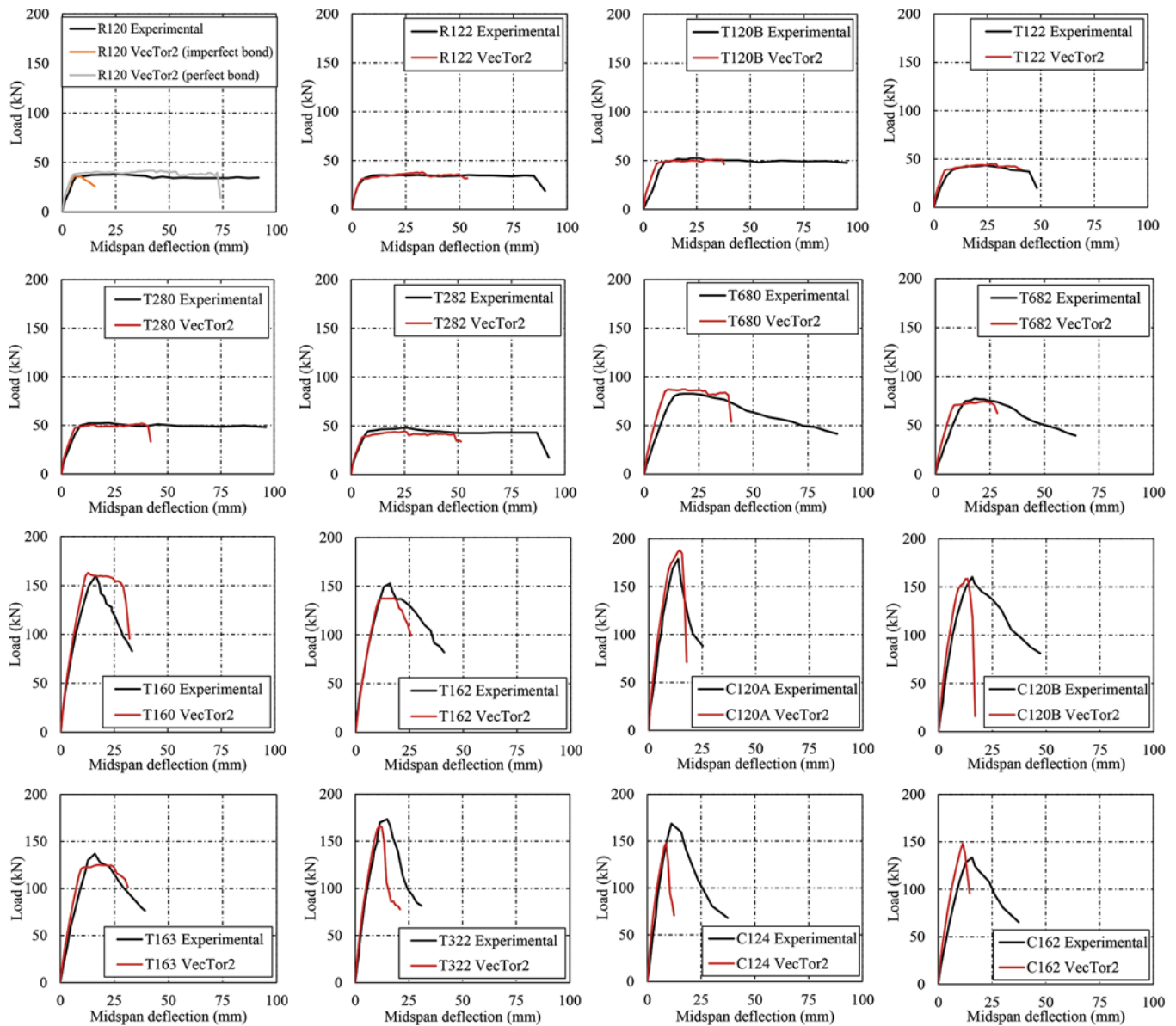


Fig. 7—Experimental versus analytical responses for Du et al.³¹ specimens. (Note: 1 kN = 225 lbf; 1 mm = 0.04 in.)

bar, measured using the gravimetric method, differed from the rest. González et al.³² found that the ratio of maximum corrosion penetration to the average value varied from 4.0 to 8.0 in naturally corroded concrete specimens. Tuutti³³ suggested that this ratio varies from 4.0 to 10.0 for 5.0 and 10.0 mm diameter reinforcing bars. It is generally accepted that the corrosion mechanism introduces a notable degree of uncertainty with respect to the structural assessment of corrosion-affected RC structures. A viable approach to address these uncertainties is stochastic FE analysis.

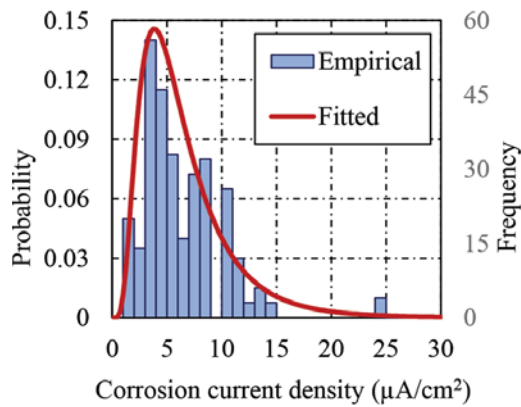
The framework required for stochastic analysis of RC elements was implemented in VecTor2 by Hunter.³⁴ The work presented herein extends these capabilities to address the uncertainties associated with corrosion.

Uniform corrosion

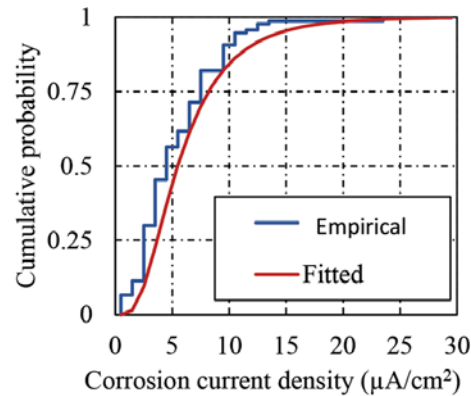
Stochastic modeling of uniform corrosion involves the definition of a probability distribution function for the corrosion rate. The corrosion rate can be treated as a single

random variable, neglecting the spatial variability, or as a random field with a prescribed covariance matrix, therefore considering spatial variability. The experimental results of Yu et al.⁴ were analyzed for the development of statistical parameters.

Yu et al.⁴ examined the spatial distribution of the reinforcing steel cross-sectional loss by testing three identical beams, Bs02, Bs03, and Bs04, which were exposed to accelerated natural corrosion for 36, 19, and 27 months, respectively. The beams were 3000 mm long and had a cross section of 280 x 150 mm. They were reinforced with two 12 mm deformed bars in tension and two 6 mm deformed bars in compression. Double-legged 6 mm diameter stirrups spaced 220 mm apart were used as the transverse reinforcement. The cross-sectional loss of the tension bars was quantified by measuring the weight loss of 10 mm pieces of reinforcing bars extracted from each beam. Although the reinforcing bars of each beam were subjected to the same



(a) Probability density function (PDF)



(b) Cumulative distribution function (CDF)

Fig. 8—Empirical and fitted PDF and CDF. (Note: 1 cm = 0.4 in.)

environment, the average and the pattern of cross-sectional loss were significantly different.

The pattern of cross-sectional loss of each beam is shown in Fig. A.12 in the Appendix section “Stochastic modeling.” The coordinates of the points of each graph were extracted, and the cross-sectional loss was converted into corrosion current density using Eq. (2). The extracted data can be found elsewhere.³⁵ The data was assumed to be part of a homogeneous isotropic random field, Z , and the graphs in Fig. A.12 were treated as six realizations of this field. A lognormal probability distribution function was fitted to the values of the corrosion current density of each realization. The fitted and the empirical probability density function (PDF) and cumulative distribution function (CDF) of the front bar of the Bs02 beam are shown in Fig. 8.

To assess the spatial correlation of the random fields, an empirical semivariogram was constructed for each realization. Because of the assumption that the realizations are isotropic, the variance was a function of distance only. The Appendix section “Stochastic modeling” details the construction of the semivariograms.

The first series of stochastic simulations was performed neglecting the spatial variability of the corrosion rate, which was modeled as a single variable in each simulation. A lognormal distribution with a mean of $150 \mu\text{A}/\text{cm}^2$ and a COV of 0.30 was used for random sampling of the corrosion current density. The COV was chosen based on the value suggested by Val et al.²⁴ and the COVs observed for the Yu et al.⁴ beams. To determine an appropriate number of simulations, the CN-50 beam was modeled 400, 200, 100, and 50 times. The loading protocol consisted of a monotonically increasing nodal displacement at the midspan with increments of 1.0 mm. The mean and COV of the failure loads and the midspan deflections at the failure load are presented in Table 5. From these values, it was concluded that 100 simulations provided sufficient accuracy for estimations of the statistical parameters. A typical plot of the stochastic simulation results is shown in Fig. 9(a). The average failure load was in good agreement with the experimentally measured one; however, there was large variability in the predicted midspan deflection at failure.

Table 5—Stochastic simulation results for CN-50 beam

	No. of simulations	400	200	100	50
Failure load, kN	Mean	74.2	73.9	75.0	73.9
	Variance	3.3	3.3	3.3	1.9
	COV, %	2.5	2.4	2.4	1.9
Midspan deflection at failure, mm	Mean	66.5	66.8	69.5	69.1
	Variance	76.2	70.0	85.6	53.5
	COV, %	13.1	12.5	13.3	10.6

Note: 1 kN = 225 lbf; 1 mm = 0.04 in.

Stochastic simulations with 100 analyses each were also performed for the CN-110, CN-210, and CN-310 beams. The COV of the failure load and the midspan deflection at failure significantly increased with the corrosion time. The statistical parameters of the failure load and the midspan deflection at failure, compared with the experimental results and the values predicted by deterministic analysis, are given in Table 6. A linear relationship was observed between the corrosion current density and the failure load. However, there was no meaningful relationship between the corrosion current density and the midspan deflection at failure.

Random field simulation of uniform corrosion was performed by employing the procedure described in the Appendix section “Stochastic modeling.” To assess the effect of the correlation length on the stochastic simulations, the CN-50 beam was modeled with four different correlation lengths: 1200, 600, 300, and 0 mm. For each correlation length, 100 simulations were performed. The statistics of the response quantities of the stochastic simulations are given in Table 7. In general, the variation in the failure load increased slightly with an increased correlation length.

Increasing the correlation length significantly increased the variation of the average and decreased the variance of a random field. Therefore, a large correlation length relative to the field length causes a smooth realization, with relatively small fluctuations around the average value. Thus, the greater variation in the failure load of the simulations with a large correlation length shows that the response of a lightly corroded RC beam is more sensitive to the average

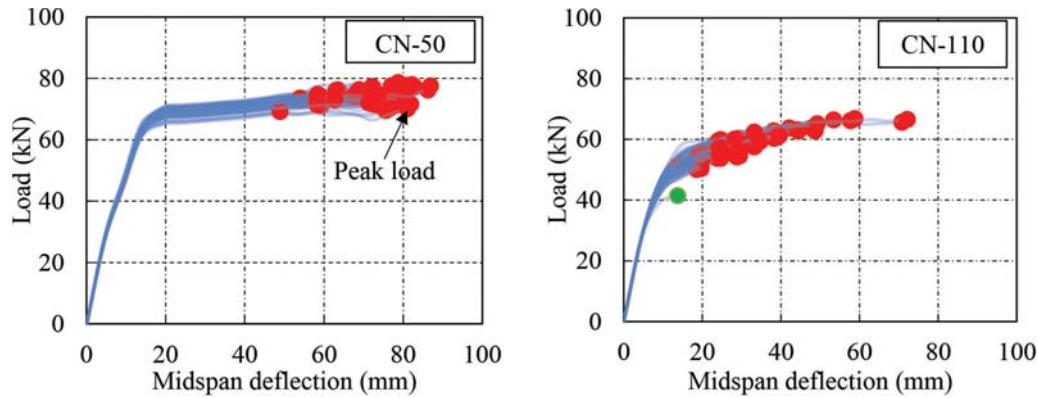


Fig. 9—Stochastic simulation results. (Note: 1 kN = 225 lbf; 1 mm = 0.04 in.)

Table 6—Stochastic simulation results

—	Beam	Stochastic		Deterministic	Experimental
		Average	COV, %		
Failure load, kN	CN-50	75.0	2.4	74.4	70.2
	CN-110	68.3	4.3	70.4	66.8
	CN-210	61.4	6.1	62.8	60.0
	CN-310	55.0	9.5	56.8	53.3
Midspan deflection, mm	CN-50	69.5	13.3	54.9	89.0
	CN-110	68.3	15.3	66.4	78.4
	CN-210	71.6	15.2	77.2	62.4
	CN-310	80.7	11.1	85.0	59.0

Note: 1 kN = 225 lbf; 1 mm = 0.04 in.

Table 7—Random field simulation results of CN-50 beam

Correlation length, mm	Failure load, kN		Midspan deflection, mm	
	Average	COV, %	Average	COV, %
0	75.2	1.4	67.7	11.0
300	74.5	2.0	67.9	10.5
600	74.7	1.9	69.0	10.4
1200	74.5	2.1	69.3	11.4

Note: 1 kN = 225 lbf; 1 mm = 0.04 in.

cross-sectional loss than the maximum loss at a locality. In conclusion, the simulation of the corrosion current density (or corrosion rate) as a random field has a negligible effect on the response. The focus should be directed toward the randomness of the average value of the corrosion current density as a single random variable, as it can be significantly different in two reinforcing bars located in the same beam and corroded under the same corrosive conditions, as illustrated in Fig. A.12 in the Appendix section “Stochastic modeling.”

Pitting corrosion

Pitting corrosion was modeled by employing the methodology proposed by Stewart and Al-Harthy.²⁰ Based on a statistical analysis of the maximum pit depth, measured over a 100 mm long corroded reinforcing bar from an accelerated

corrosion test, Stewart and Al-Harthy²⁰ proposed a Gumbel distribution for the pitting factor.

The beams tested by El Maaddawy et al.³⁰ were modeled again; for every corroded truss element, a random pitting factor was generated, and the cross-sectional loss due to pitting corrosion of the corroded truss elements was calculated based on the formulations presented in the “Corrosion rate” section. In addition to the reduction of the reinforcement cross-sectional area, degradation due to pitting corrosion of mechanical properties such as the yield strength was implemented in the FE models by the formulations summarized previously.

Stochastic simulation results for the CN-110 beam are shown in Fig. 9(b). Compared with uniform corrosion, a significantly larger scatter in the failure load and the midspan deflection at failure can be observed. The average and COV of the failure load and the midspan deflection are given in Table 8 for all the specimens. The failure load and the midspan deflection decreased with the increase of the maximum pitting factor.

The response of the CN-310 beam was significantly different from that of the other beams mainly because it was governed by the rupture of the tension reinforcement. For this beam, the ultimate strain of almost every corroded truss element was reduced by 70%. An average cross-sectional loss of 50% was also calculated. As a result, the failure load was reduced from 55.0 kN (the average of uniform corrosion simulations) to 5.3 kN, showing the devastating effect of

pitting corrosion. Although such a reduction might be purely hypothetical, it highlights the important areas of study for stochastic FE modeling of pitting corrosion.

The datum point in green in Fig. 9(b) shows the possibility of an ultimate midspan deflection of less than 20 mm for a beam that could reach a 72 mm deflection at the midspan with a different pitting corrosion scenario. The failure in such a case, depicted in Fig. 10, is governed by pitting factors much greater than the average pitting factor in the areas shown. Taking a minimum midspan deflection of 20 mm as a defined limit state, the stochastic analysis undertaken in this study shows a 13% probability of failure to meet such a condition after 110 days of corrosion.

RECOMMENDATIONS FOR FUTURE WORK

The main objective of this work was to develop and verify a numerical procedure for modeling and assessing corrosion-damaged RC elements. In doing so, some limitations were found that stem from the constitutive models currently available in the literature. The following recommendations are made for further improving the computational capabilities:

1. The discrepancy between the applied and achieved corrosion current density in accelerated corrosion tests needs to be further studied. Potential inaccuracy in the primary input parameter of corrosion damage models can lead to significant errors.

2. Additional work must be undertaken to investigate the type of corrosion products under different environmental conditions; the corrosion-induced tensile strains in concrete and the time to cracking are severely affected by the type of corrosion products.

3. Experimental evidence suggests that both uniform and pitting corrosion occur at the same time. Thus, it is of interest to develop a hybrid corrosion model that combines the effects of simultaneous pitting and uniform corrosion. Such a model can potentially generate a more realistic representation of the corrosion pattern of a reinforcing bar.

Table 8—Stochastic simulation results for pitting corrosion

Beam	Failure load, kN		Midspan deflection, mm	
	Average	COV, %	Average	COV, %
CN-50	77.1	1.4	73.5	11.1
CN-110	57.8	6.7	29.5	35.7
CN-210	31.1	21.6	16.2	40.2
CN-310	12.8	17.1	5.31	42.7

Note: 1 kN = 225 lbf; 1 mm = 0.04 in.

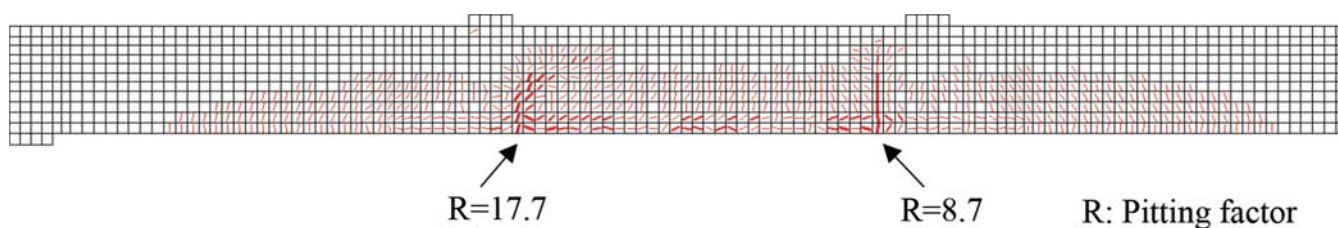


Fig. 10—Failure pattern in simulation with largest pitting factors.

4. A statistical distribution, quantifying the probability of pitting corrosion at a certain location along the length of a reinforcing bar, would be a valuable asset to the stochastic modeling of corrosion. The assumption that a pit forms over every corroded truss element, made in the analyses performed in this work, should be regarded as the worst-case scenario.

CONCLUSIONS

The work presented in this paper included the implementation and development of corrosion damage models within the nonlinear finite element (FE) analysis program VecTor2. The validation studies performed investigated the influence of various behavioral mechanisms on the structural response, as well as the suitability of stochastic analysis to address the high level of uncertainties with respect to the material properties of corrosion-damaged elements. Although the program is primarily a two-dimensional (2-D) FE analysis program with limited three-dimensional (3-D) capabilities, implementing the developed models into a 3-D framework would be similarly straightforward.

Based on the results obtained from the deterministic and stochastic modeling of corroded reinforced concrete (RC) beams, the following conclusions and observations were made:

1. FE modeling employing a smeared rotating crack concept for RC provides a convenient and reliable framework for incorporating corrosion-induced mechanisms into the analysis of RC structures.

2. The approach developed herein, with the Distributed Stress Field Model as a basis, is found to model the stiffness, strength, ductility, and failure mode of corroded RC members with reasonable accuracy.

3. The most influential factor affecting the strength of an RC beam suffering from corrosion is the corrosion rate (that is, the reduction of the reinforcement cross-sectional area).

4. The bond strength degradation of corroded reinforcing bars is also an important mechanism influencing the structural response. A significant slip was calculated for most of the corroded beams analyzed.

5. Cracking of the concrete cover had a negligible effect on the calculated response of the corroded specimens. Nevertheless, this mechanism may be key for a serviceability limit state.

6. The statistics of the response quantities of RC beams damaged by uniform corrosion are accurately estimated by modeling the rate of corrosion as a single random variable rather than a random field. Consideration of the spatial variability of the rate of corrosion does not lead to a significantly different response.

7. The strength reduction of a corroded beam is more severe when pitting corrosion is present, compared with uniform corrosion.

8. For the beams subjected to pitting corrosion, the flexural strength is highly sensitive to the maximum pitting factor.

9. Stochastic analyses revealed a large variation in the calculated responses based on the location and severity of the pitting corrosion.

AUTHOR BIOS

Siavash Habibi is a Structural Engineer at AJW Engineering in Toronto, Canada. He received his MASC from the University of Toronto, ON, Canada, and his BAsC from the University of Tehran, Tehran, Iran. His research interests include the structural implications of corrosion and stochastic finite element analysis of corrosion-affected reinforced concrete structures.

Anca C. Ferche is an Assistant Professor in the Department of Civil, Architectural and Environmental Engineering at The University of Texas at Austin, Austin, TX. She received her PhD from the University of Toronto in 2020. Her research interests include performance assessment and analysis of reinforced concrete structures, concrete deterioration mechanisms, and rehabilitation of structures.

Frank J. Vecchio, F.A.C.I., is a Professor in the Department of Civil and Mineral Engineering at the University of Toronto. He is a past member of Joint ACI-ASCE Committees 441, Reinforced Concrete Columns, and 447, Finite Element Analysis of Reinforced Concrete Structures. He is a recipient of the 1998 ACI Structural Research Award, the 1999 Structural Engineering Award, the 2011 Wason Medal for Most Meritorious Paper, the 2016 Joe W. Kelly Award, and the 2020 Arthur J. Boase Award. His research interests include advanced constitutive modeling and analysis of reinforced concrete, and assessment and rehabilitation of structures.

ACKNOWLEDGMENTS

The authors would like to acknowledge IC-IMPACTS for the primary funding support provided to this project. The authors would also like to acknowledge the Natural Sciences and Engineering Research Council of Canada for its contributions.

REFERENCES

1. Federation of Canadian Municipalities (FCM), "Monitoring the State of Canada's Core Public Infrastructure (Canadian Infrastructure Report Card 2019)," 2019, 56 pp., canadainfrastructure.ca. (last accessed December 23, 2021)
2. ASCE, "A Comprehensive Assessment of America's Infrastructure (2017 Infrastructure Report Card)," American Society of Civil Engineers, Reston, VA, 2017, 112 pp., infrastructurereportcard.org. (last accessed December 23, 2021)
3. Böhni, H., *Corrosion in Reinforced Concrete Structures*, Woodhead Publishing, Sawston, UK, 2005, 264 pp.
4. Yu, L.; Francois, R.; Dang, V. H.; L'Hostis, V.; and Gagne, R., "Distribution of Corrosion and Pitting Factor of Steel in Corroded RC Beams," *Construction and Building Materials*, V. 95, Oct. 2015, pp. 384-392. doi: 10.1016/j.conbuildmat.2015.07.119
5. Wang, X. H., and Liu, X. L., "Modelling Effects of Corrosion on Cover Cracking and Bond in Reinforced Concrete," *Magazine of Concrete Research*, V. 56, No. 4, May 2004, pp. 191-199. doi: 10.1680/mac.2004.56.4.191
6. Bhargava, K.; Ghosh, A. K.; Mori, Y.; and Ramanujam, S., "Corrosion-Induced Bond Strength Degradation in Reinforced Concrete—Analytical and Empirical Models," *Nuclear Engineering and Design*, V. 237, No. 11, June 2007, pp. 1140-1157. doi: 10.1016/j.nucengdes.2007.01.010
7. Cairns, J.; Plizzari, G. A.; Du, Y.; Law, D. W.; and Franzoni, C., "Mechanical Properties of Corrosion-Damaged Reinforcement," *ACI Materials Journal*, V. 102, No. 4, July-Aug. 2005, pp. 256-264.
8. VecTor Analysis Group, "Nonlinear Finite Element Analysis Software for Reinforced Concrete Structures," VTAG, 2020, vectoranalysisgroup.com. (last accessed November 19, 2021)
9. Wong, P. S.; Vecchio, F. J.; and Trommels, H., "VecTor2 and FormWorks User's Manual (Technical Report)," Department of Civil Engineering, University of Toronto, Toronto, ON, Canada, Aug. 2013, 347 pp.
10. Vecchio, F. J., and Collins, M. P., "The Modified Compression-Field Theory for Reinforced Concrete Elements Subjected to Shear," *ACI Journal Proceedings*, V. 83, No. 2, Mar.-Apr. 1986, pp. 219-231.
11. Vecchio, F. J., "Disturbed Stress Field Model for Reinforced Concrete: Formulation," *Journal of Structural Engineering*, ASCE, V. 126, No. 9, Sept. 2000, pp. 1070-1077. doi: 10.1061/(ASCE)0733-9445(2000)126:9(1070)
12. Otieno, M.; Beushausen, H.; and Alexander, M., "Prediction of Corrosion Rate in RC Structures—A Critical Review," *Modelling of Corroding Concrete Structures*, V. 5, C. Andrade, and G. Mancini, eds., RILEM Bookseries, Springer, Dordrecht, the Netherlands, 2011, pp. 15-37.
13. Alonso, C.; Andrade, C.; and González, J. A., "Relation between Resistivity and Corrosion Rate of Reinforcements in Carbonated Mortar Made with Several Cement Types," *Cement and Concrete Research*, V. 18, No. 5, Sept. 1988, pp. 687-698. doi: 10.1016/0008-8846(88)90091-9
14. Bazant, Z. P., "Physical Model for Steel Corrosion in Concrete Sea Structures—Theory," *Journal of the Structural Division*, ASCE, V. 105, No. 6, June 1979, pp. 1137-1153. doi: 10.1061/JSDEAG.0005168
15. Andrade, C.; Alonso, C.; and Molina, F. J., "Cover Cracking as a Function of Rebar Corrosion: Part I—Experimental Test," *Materials and Structures*, V. 26, No. 8, Oct. 1993, pp. 453-464. doi: 10.1007/BF02472805
16. Liu, Y., and Weyers, R. E., "Modeling the Time-to-Corrosion Cracking in Chloride Contaminated Reinforced Concrete Structures," *ACI Materials Journal*, V. 95, No. 6, Nov.-Dec. 1998, pp. 675-681.
17. Andrade, C.; Alonso, C.; González, J. A.; and Rodriguez, J., "Remaining Service Life of Corroding Structures," *Proceedings, IABSE Symposium on Durability of Structures*, Lisbon, Portugal, Sept. 1989, pp. 359-363.
18. Rodriguez, J.; Ortega, L. M.; and Casal, J., "Load Carrying Capacity of Concrete Structures with Corroded Reinforcement," *Construction and Building Materials*, V. 11, No. 4, June 1997, pp. 239-248. doi: 10.1016/S0950-0618(97)00043-3
19. El Maaddawy, T. A., and Soudki, K. A., "Effectiveness of Impressed Current Technique to Simulate Corrosion of Steel Reinforcement in Concrete," *Journal of Materials in Civil Engineering*, ASCE, V. 15, No. 1, Feb. 2003, pp. 41-47. doi: 10.1061/(ASCE)0899-1561(2003)15:1(41)
20. Stewart, M. G., and Al-Harthy, A., "Pitting Corrosion and Structural Reliability of Corroding RC Structures: Experimental Data and Probabilistic Analysis," *Reliability Engineering & System Safety*, V. 93, No. 3, Mar. 2008, pp. 373-382. doi: 10.1016/j.res.2006.12.013
21. Pantazopoulou, S. J., and Papoulia, K. D., "Modeling Cover-Cracking due to Reinforcement Corrosion in RC Structures," *Journal of Engineering Mechanics*, ASCE, V. 127, No. 4, Apr. 2001, pp. 342-351. doi: 10.1061/(ASCE)0733-9399(2001)127:4(342)
22. Val, D. V.; Chernin, L.; and Stewart, M. G., "Experimental and Numerical Investigation of Corrosion-Induced Cover Cracking in Reinforced Concrete Structures," *Journal of Structural Engineering*, ASCE, V. 135, No. 4, Apr. 2009, pp. 376-385. doi: 10.1061/(ASCE)0733-9445(2009)135:4(376)
23. Al-Sulaimani, G. J.; Kaleemullah, M.; Basunbul, I. A.; and Rash-eeduzzafar, "Influence of Corrosion and Cracking on Bond Behavior and Strength of Reinforced Concrete Members," *ACI Structural Journal*, V. 87, No. 2, Mar.-Apr. 1990, pp. 220-231.
24. Val, D. V.; Stewart, M. G.; and Melchers, R. E., "Effect of Reinforcement Corrosion on Reliability of Highway Bridges," *Engineering Structures*, V. 20, No. 11, Nov. 1998, pp. 1010-1019. doi: 10.1016/S0141-0296(97)00197-1
25. Chung, L.; Cho, S.-H.; Jay Kim, J.-H.; and Yi, S.-T., "Correction Factor Suggestion for ACI Development Length Provisions Based on Flexural Testing of RC Slabs with Various Levels of Corroded Reinforcing Bars," *Engineering Structures*, V. 26, No. 8, July 2004, pp. 1013-1026. doi: 10.1016/j.engstruct.2004.01.008
26. Feng, Q.; Visintin, P.; and Oehlers, D. J., "Deterioration of Bond-Slip due to Corrosion of Steel Reinforcement in Reinforced Concrete," *Magazine of Concrete Research*, V. 68, No. 15, Aug. 2016, pp. 768-781. doi: 10.1680/jmacr.15.00217
27. El Maaddawy, T.; Soudki, K.; and Topper, T., "Analytical Model to Predict Nonlinear Flexural Behavior of Corroded Reinforced Concrete Beams," *ACI Structural Journal*, V. 102, No. 4, July-Aug. 2005, pp. 550-559.
28. Du, Y., "Effect of Reinforcement Corrosion on Structural Concrete Ductility," PhD dissertation, University of Birmingham, Birmingham, UK, 2001, 320 pp.
29. Azad, A. K.; Ahmad, S.; and Azher, S. A., "Residual Strength of Corrosion-Damaged Reinforced Concrete Beams," *ACI Materials Journal*, V. 104, No. 1, Jan.-Feb. 2007, pp. 40-47.
30. El Maaddawy, T.; Soudki, K.; and Topper, T., "Long-Term Performance of Corrosion-Damaged Reinforced Concrete Beams," *ACI Structural Journal*, V. 102, No. 5, Sept.-Oct. 2005, pp. 649-656.
31. Du, Y.; Clark, L. A.; and Chan, A. H. C., "Impact of Reinforcement Corrosion on Ductile Behavior of Reinforced Concrete Beams," *ACI Structural Journal*, V. 104, No. 3, May-June 2007, pp. 285-293.

32. González, J. A.; Andrade, C.; Alonso, C.; and Feliu, S., "Comparison of Rates of General Corrosion and Maximum Pitting Penetration on Concrete Embedded Steel Reinforcement," *Cement and Concrete Research*, V. 25, No. 2, Feb. 1995, pp. 257-264. doi: 10.1016/0008-8846(95)00006-2

33. Tuutti, K., "Corrosion of Steel in Concrete," Swedish Cement and Concrete Research Institute, Stockholm, Sweden, 1982, 472 pp.

34. Hunter, M. D., "Towards Stochastic Finite Element Analysis of Reinforced Concrete Structures," MSc thesis, University of Toronto, Toronto, ON, Canada, 2016, 281 pp.

35. Habibi, S., "Finite Element Modelling of Corrosion Damaged Reinforced Concrete Structures," MSc thesis, University of Toronto, Toronto, ON, Canada, 2017, 157 pp.

36. Krajewski, W. F., "Estimation of the Covariance and Semivariogram for Stationary, Isotropic Random Fields," *Proceedings*, Budapest Symposium, Integrated Design of Hydrological Networks, IAHS Publication No. 158, Budapest, Hungary, 1986, pp. 71-84.